Chemical Engineering Journal 403 (2021) 126335

Contents lists available at ScienceDirect

Chemical Engineering Journal

journal homepage: www.elsevier.com/locate/cej

Mechanistic modelling of wastewater disinfection by the photo-Fenton process at circumneutral pH

Cintia Casado[a], José Moreno-SanSegundo[a], Irene De la Obra[b,c], Belén Esteban García[b,c], José Antonio Sánchez Pérez[b,c], Javier Marugán[a,*]

[a] Department of Chemical and Environmental Technology, ESCET, Universidad Rey Juan Carlos, C/Tulipán s/n, 28933 Madrid, Spain
[b] Solar Energy Research Centre (CIESOL), Joint Centre University of Almería-CIEMAT, Carretera de Sacramento s/n, E-04120 Almería, Spain
[c] Chemical Engineering Department, University of Almería, Ctra de Sacramento s/n, E-04120 Almería, Spain

HIGHLIGHTS

- Mechanistic modelling of *E. coli* inactivation by photo-Fenton at circumneutral pH.
- Radiation transport considering optical properties of iron hydroxide precipitates.
- Reversible *serial n-event* kinetic model successfully describes solar inactivation.
- Photo-Fenton cycle mediated by precipitated iron reproduces *photosaturation* effect.
- *Multiple target – multiple hit* model reproduces synergy of photons and radicals.

ARTICLE INFO

Keywords:
Kinetic modelling
Escherichia coli
Optical properties
Serial event
Multiple target – multiple hit

ABSTRACT

This work focuses, for the first time, on the mechanistic modelling of wastewater disinfection by the solar photo-Fenton process using controlled solar simulated radiation. At circumneutral pH, iron precipitates forming hydroxides and significantly affecting the optical properties of the water. In this regard, radiation transfer in the reactor has been taken into account. The proposed model considers that the solar inactivation of bacteria follows a *serial n-event* mechanism with *n* reversible steps of photonic attacks leading to the bacterial inactivation. Dark Fenton cyclic process of hydroxyl radical formation from hydrogen peroxide is considered to be mediated mainly by precipitated iron species, prevailing at circumneutral pH. Finally, the photo-Fenton process was modelled using a *multiple target – multiple hit* mechanistic approach that accounts for the synergistic effect between the photonic and the hydroxyl radical attacks to the bacteria. Model predictions successfully reproduce experimental data of solar disinfection, hydrogen peroxide consumption, and photo-Fenton disinfection at circumneutral pH.

1. Introduction

The discharge of municipal wastewater treatment plant (MWWTP) effluents is a serious environmental problem due to, among other issues, the high load of microorganisms, including pathogens that can provoke infections in plants, animals and humans. Therefore, the disinfection of these effluents is absolutely required to avoid environmental problems and/or for water reclamation purposes. Solar photo-Fenton is a disinfection technology effective against microorganisms due to the combined effect of the direct action of solar photons and the photoactivated generation of hydroxyl radicals from hydrogen peroxide catalysed by iron species. Although it is well-know that the optimal pH for Fenton processes is around 2.8 [1], when large volumes of water, such as MWWTP effluents, have to be treated, operation at neutral pH is proposed to avoid costs related to pH conditioning. Therefore, as these effluents present near neutral pH, the addition of iron salts leads to its fast precipitation, being the iron hydroxides the initiators of the heterogeneous photo-Fenton process in water disinfection processes at this pH range [2].

Since the early works of Chick [3] and Watson [4], various rate expressions have been proposed for the kinetic modelling of disinfection processes. The simple Chick-Watson model considers a first-order inactivation process that predicts a log-linear decrease of viable microorganism with time. Therefore, this model is not able to describe different regions in experimental disinfection curves, such as an initial delay or *shoulder*, or a final deceleration or *tail* at the end of the

* Corresponding author.
E-mail address: javier.marugan@urjc.es (J. Marugán).

https://doi.org/10.1016/j.cej.2020.126335
Received 17 May 2020; Received in revised form 26 June 2020; Accepted 16 July 2020
Available online 22 July 2020

reaction, being required further mechanistic considerations [5–8]. More complex mathematical models were developed to represent the dose-response behaviour observed when a microbial population is exposed to a disinfectant [9], representing disinfection as a permanent variation in the population resistance. Some examples are the use of: i) empirical *probabilistic models* [10] based on the use of probability functions to describe the distribution of inactivation times for a population of organisms considering specific sensitivities to a certain level of disinfectant exposure; ii) the *serial n-event* model [11,12], in which the inactivation takes place through a sequence of discrete damage levels and the organism is assumed to be inactivated after a threshold level of damage; iii) the *multi-target model* [11], similar to the *series-event model* but assuming that each organism contains a finite number of discrete critical targets, each of which must be attacked for full inactivation; and iv) the *Hass* model [13], formulated on chemical reaction principles, but assuming the existence of an intermediary organism-disinfectant complex.

Despite the extensive literature on the evaluation of photo-Fenton processes for the inactivation of microorganisms at circumneutral pH [14–21], most of these studies focused on the qualitative analysis of experimental data, and only few of them include some basic kinetic analysis, usually by fitting the results to the semi-empirical Chick-Watson model, whose prediction capabilities outside the exact experimental setup and operational conditions in which has been calculated is very limited. Some mechanistic approaches have been reported for the kinetic modelling of TiO_2 photocatalytic disinfection [22] or solar water disinfection [23,24] processes. However, to the best of the authors' knowledge, there are no reports in the literature about the mechanistic modelling of photo-Fenton disinfection processes, either in acidic or circumneutral conditions. Some kinetic modelling approaches have been applied to the photo-Fenton oxidation at acidic pH of chemical pollutants such as paracetamol [25], acetamiprid (ACTM) and thiabendazole (TBZ) [26], and for the determination of the intrinsic kinetic constants of the photo-Fenton reaction at circumneutral pH using the soluble complex Fe^{3+}-EDDS [27].

The aim of this work is the rigorous mechanistic modelling of the photo-Fenton inactivation of microorganisms at circumneutral pH, in which the activation takes place in the heterogeneous phase constituted by the iron hydroxides precipitates. To determine the intrinsic kinetics parameters of the radiation activation step, the optical properties of the suspension have been calculated from spectrophotometric measurements. The estimated absorption and scattering coefficients of the suspensions have been used for the resolution of the radiation transport in the water media, allowing an accurate calculation of the incident radiation profiles. An innovative *multiple target – multiple hit* mechanistic modelling approach has been applied for the successful description of the synergistic effect of the direct solar inactivation and the hydroxyl radical mediated Fenton process during the photo-Fenton disinfection of MWWTP effluents.

2. Materials and methods

2.1. Reagents and analytical determinations

Two different concentrations of iron were used (10 and 20 mg L^{-1} of Fe), with ferrous sulphate heptahydrate ($FeSO_4{\cdot}7H_2O$, 99%, Panreac, Spain) as source of iron. The concentration was analysed by the o-phenantroline standardized method according to ISO 6332 with a limit of detection of 0.5 mg L^{-1}. Hydrogen peroxide (33%, w/v aqueous solution, Panreac, Spain) concentration was analysed by a colourimetric method (DIN 38 402 H15) using titanium (IV) oxysulphate (98%, Sigma-Aldrich, Spain) with a limit of detection of 0.3 mg L^{-1}.

2.2. Bacterial enumeration and quantification

Escherichia coli K-12 ATCC 23631 was inoculated from a stock suspension into Luria broth nutrient medium (Miller's LB Broth, Sigma–Aldrich, USA) and incubated at 37 °C with constant agitation in a rotary shaker under aerobic conditions. Bacteria were collected after 20 h of incubation, corresponding to the initial bacterial stationary phase, yielding a concentration of 10^9 CFU mL^{-1}. *E. coli* suspensions were harvested by centrifugation at 3000 rpm for 10 min. Finally, the bacterial pellet was re-suspended in phosphate buffer saline solution (PBS) and diluted in the reactor to the required 10^6 CFU mL^{-1} cell density initial concentration. Colonies were counted after incubation of 24 h at 37 °C, as described elsewhere [28]. The concentration of *E. coli* in water was measured using the plate counting technique. 50–100–250–500–1000 μL of samples were plated out to reach the detection limit (DL), 1 CFU mL^{-1}.

2.3. Water matrix

To avoid the variability in real wastewater effluent, the experiments were carried out at pH 7 using a simulated MWWTP effluent (SMWWTPE) with 15 mg L^{-1} of total inorganic carbon (TIC) added as sodium bicarbonate ($NaHCO_3$) [21,26]. The constituents of the SMWWTPE were: $CaSO_4{\cdot}2H_2O$ (60 mg L^{-1}), $MgSO_4$ (60 mg L^{-1}), KCl (4 mg L^{-1}), $(NH_4){\cdot}2SO_4$ (23.6 mg L^{-1}), beef extract (1.8 mg L^{-1}), peptone (2.7 mg L^{-1}), humic salts (4.2 mg L^{-1}), sodium lignin sulfonate (2.4 mg L^{-1}), sodium lauryle sulphate (0.9 mg L^{-1}), acacia gum powder (4.7 mg L^{-1}), arabic acid (5.0 mg L^{-1}) and $NaHCO_3$ (105 mg L^{-1}). The dissolved organic carbon concentration (DOC) was 9 mg L^{-1}.

2.4. Experimental setup

2.4.1. Disinfection

Photo-Fenton experiments were carried out in a jacketed cylindric stirred tank reactor (10 cm internal diameter) which allowed to control the water temperature at 25 °C using a thermostatic bath (Thermo Scientific Neslab RTE 7), placed inside a solar simulator (SunTest CPS + from Atlas). Fig. S.1 compares the emission of the solar simulator with the ASTM G173 AM 1.5 standard solar spectrum. The total working volume was 0.35 L (5 cm of liquid depth). The irradiation on reactor surface was monitored during the experiments by a spectroradiometer (AvantesAvaSpec-ULS204).

The selected operation conditions were: 30 mg L^{-1} of initial concentration of hydrogen peroxide, 10^6 CFU mL^{-1} of *E. coli* initial concentration, two initial iron concentrations (10 and 20 mg L^{-1}) and several UVA irradiation levels (between 10 and 50 W m^{-2}) adjusted by the intensity control in the front panel of the simulator and measured with the spectroradiometer. All the experiments were carried out in triplicate.

The reactor was filled with the SMWWTPE. The heterogeneous photo-Fenton reaction started when both, reagents and bacterial suspension, were added in the reactor and were exposed to simulated sunlight. Water samples were taken at short time intervals to evaluate H_2O_2 consumption and *E. coli* inactivation, in the latter case upon addition of catalase to remove H_2O_2 from the samples. Besides, control tests were performed evaluating the individual effects of radiation, hydrogen peroxide, mechanical stress and iron. Experiments of direct solar inactivation were carried out under the same experimental conditions without addition of iron and H_2O_2.

2.4.2. Optical properties determination

To study the optical properties of iron precipitates, a spectrophotometer (Varian Cary 500 Scan UV–VIS-NIR) with an integrating sphere diffuse reflectance accessory was used. The calculation of the optical properties is a complex task when both absorption and dispersion phenomena occur simultaneously. While the extinction coefficient can be calculated easily through the normal use of a spectrophotometer, additional measurement of diffuse transmission and reflectance are required to obtain both the absorption and dispersion coefficients

[29,30]. An integrating sphere of 110 mm in diameter coated with PTFE and a cell of 1 cm of optical pathway were used. A schematic representation of the experimental setup can be found elsewhere [30]. The spectral absorption and scattering coefficients in the UV-A wavelength range were calculated by fitting the experimental data of direct and diffuse transmission of the suspensions to the transmitted and reflected radiation fluxes. These fluxes were calculated by resolution of the radiative transfer equation in the cell using a 1-D discrete ordinate method assuming an isotropic scattering phase function by means of a nonlinear multiparameter regression algorithm. Duplicated experimental data were obtained for different initial concentrations of Fe (10, 15, 20 and 25 mg L^{-1}) in SMWWTPE with 30 mg L^{-1} of hydrogen peroxide in a recirculated well-mixed system.

2.5. Calculation of kinetic parameters

Rigorous kinetic description of the photo-Fenton process requires the explicit inclusion in the model of the photon absorption rate. The value of the incident radiation (G, W m^{-2}) was first calculated considering the spectral distribution of absorption, scattering and emission in the UVA range by solving the radiative transfer equation as follows:

$$\frac{dI_{\lambda,\underline{\Omega}}}{dh} = -\kappa_\lambda I_{\lambda,\underline{\Omega}} - \sigma_\lambda I_{\lambda,\underline{\Omega}} + \frac{\sigma_\lambda}{4\pi}\int_{\Omega'=4\pi} p(\underline{\Omega}' \rightarrow \underline{\Omega}) I_{\lambda,\Omega'} d\Omega' \quad (1)$$

$$G_{\lambda(h)} = \int_{\Omega=0}^{\Omega=4\pi} I_\lambda(\Omega) d\Omega \quad (2)$$

$$G = \langle G_{\lambda(h)} \rangle = \sum_{\lambda\,\min}^{\lambda\,\max} \frac{\int_0^H G_{\lambda(h)} \cdot dh}{\int_0^H dH} \quad (3)$$

where $I_{\lambda,\underline{\Omega}}$ is the intensity of photons with wavelength λ propagated along the direction $\underline{\Omega}$;κ_λ is the volumetric absorption coefficient, σ_λ is the volumetric scattering coefficient and $p(\underline{\Omega}' \rightarrow \underline{\Omega})$ is the phase function that describes the directional distribution of scattered radiation. A spatial step of 0.025 cm was used to discretise the 5 cm of water depth in the reactor. Bacterial absorption can be neglected from the radiation transport viewpoint.

The rate of an elementary photoactivated reaction (r, mol L^{-1} s^{-1}) can be expressed as the product of the quantum yield of the reaction (ϕ, mol Einstein^{-1}) and the volumetric rate of photon absorption, VRPA (e^a, Einstein L^{-1} s^{-1}), i.e:

$$A \xrightarrow{h\upsilon} B \qquad r_A = \phi\, e_A^a$$

The averaged volumetric rate of photon absorption (VRPA) for each experiment can be calculated by multiplying the spectral averaged absorption coefficient by the incident radiation.

$$VRPA_A = e_A^a = \kappa_A G = \kappa_A^* [A] G \quad (4)$$

where κ_A^* is the spectral averaged specific volumetric absorption coefficient of reactant A. As the quantum yield and the specific absorption coefficient are constant, they can be grouped into a new kinetic parameter to simplify the rate expressions as:

$$A \xrightarrow{h\upsilon} B \qquad r_A = k[A]G$$

where the kinetic constant k (m^2 J^{-1}) acts as a second-order kinetic constant with regards to the concentration of the reactant and the incident radiation.

Calculation of the kinetic parameters was carried out by minimizing the normalized root mean squared logarithmic error (NRMSLE) between the experimental and predicted concentration of viable bacteria concentration (for bacterial inactivation) and the normalized root mean squared error (NRMSE) for H_2O_2 consumption profiles. The sequential quadratic programming (SQP) optimization method from GNU Octave was used to minimize the objective error function. The system of differential equations was solved using explicit Euler. An independence analysis was carried out to achieve a value of the time step low enough.

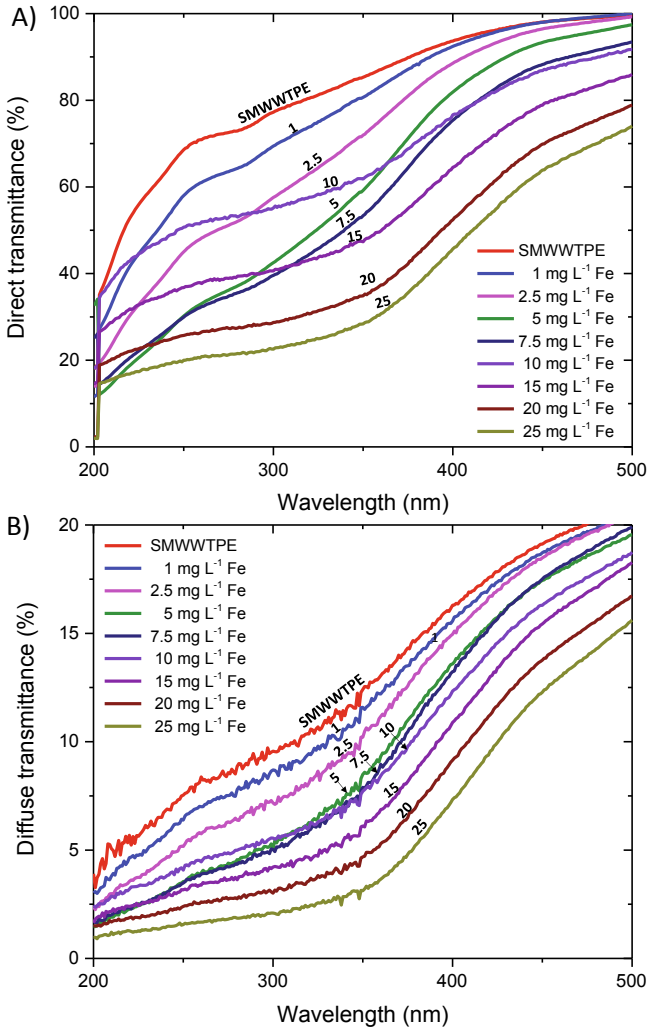

Fig. 1. Optical measurements for different suspension of iron in SMWWTPE with carbonates at neutral pH: A) Direct transmittance, B) Diffuse transmittance.

3. Results and discussion

3.1. Optical properties

Experimental data of direct and diffuse transmittance for the SMWWTPE with different concentrations of Fe are shown in Fig. 1. Results of direct transmittance in Fig. 1A clearly show the existence of two different sets of curve trends depending on the iron concentration level. Up to 7.5 mg L^{-1}, a clear decrease in transmission is observed as the concentration increases, as expected for the higher radiation extinction by these low-turbidity suspensions. In contrast, above this value a second region starts in which iron hydroxide becomes the predominant species, leading to much higher turbidity in the suspension. In fact, the massive formation of solids at 10 and 15 mg L^{-1} of iron decreases the extinction of the suspensions with regards to 7.5 mg L^{-1}, especially for shorter wavelengths. This effect suggests that the increase in scattering by the particles in suspension does not counteract the decrease in absorption due to the disappearance of the homogeneous iron species from the solution. For higher concentrations of iron, the expected decrease in transmission takes place again, showing two different shapes of the spectra depending on the iron concentration range that can be concluded to be related to the predominance of

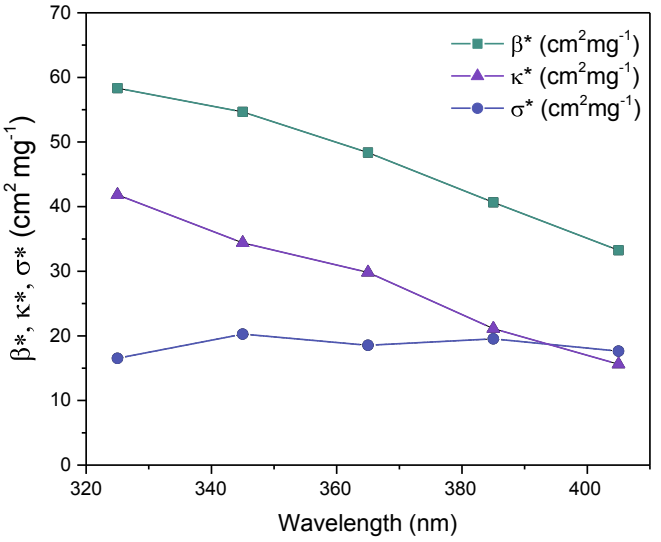

Fig. 2. Optical properties of the iron suspensions as a function of irradiance wavelength. Spectral specific extinction (β^*_λ), scattering (σ^*_λ) and absorption (κ^*_λ) coefficients. The numerical values of the coefficients are available in Table S.1.

soluble or insoluble iron species. A similar effect is also observed in the diffuse transmittance results (Fig. 1B), although in this case, the differences between both regions are less pronounced. The net effect is that the radiation transmission observed with 5 mg L^{-1} and 10 mg L^{-1} of Fe is very similar, with a significant contribution of the diffuse transmission. In contrast, diffuse reflectance values (data not shown) were very small, below 5% in all measurements and without clear trends, being neglected in the calculations.

Fig. 2 shows the calculated spectral extinction (β_λ), scattering (σ_λ) and absorption (κ_λ) coefficients in the wavelength range from 325 nm to 405 nm for the suspension in the region of higher concentration of iron where iron hydroxides are the predominant species. The reason is that this is the iron concentration range where the photo-Fenton processes for the treatment of MWWTP effluent usually operate [31,32]. Whereas the scattering coefficient remained essentially constant independently of the wavelength, the absorption coefficient diminished as the wavelength increased, as occurred with the extinction coefficient.

3.2. Modelling of direct solar inactivation of microorganisms

Fig. 3**A** presents the results of the effect of UV irradiance, I_{UV} (W m^{-2}), on the bacterial inactivation in a simulated MWWTP effluent at circumneutral pH by direct solar disinfection. After 120 min of reaction, a 3-log decay was obtained with the higher irradiance of 50 W m^{-2} and 2.5-log for 30 W m^{-2}. For irradiance values below 30 W m^{-2} (25–10 W m^{-2}), negligible bacterial inactivation was observed under the studied conditions of controlled temperature at 25 °C and no additional stress factors. Fig. 3**B** shows these results plotted as a function of the UV dose. It can be noticed that the curves do not overlap, meaning that the results depend on the power and not only on the accumulated energy as happens for the removal of chemical contaminants. For instance, for the same dose of 1100 kJ m^{-2}, higher damage in bacterial population is obtained when high UV irradiance values are applied in shorter times. Although solar photo-inactivation processes for water disinfection have proven to be more efficient when a higher solar energy dose is received in the system [33], there is not a simple relationship between microorganism photo-inactivation rate and solar exposure time, energy received, or dose applied [15]. In the

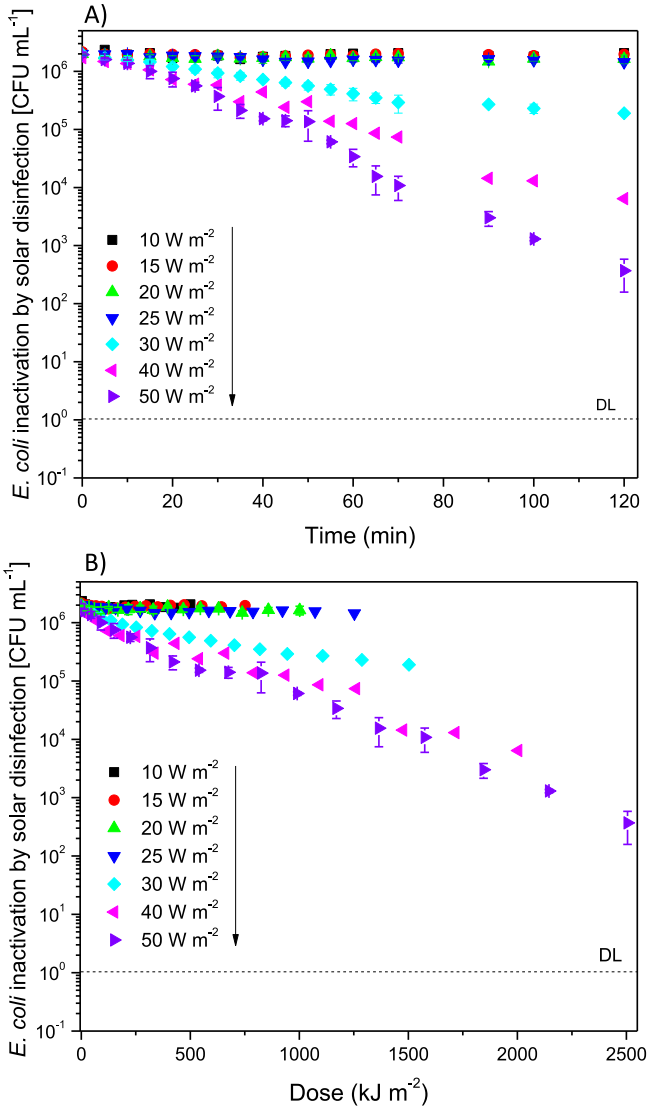

Fig. 3. Experimental results of bacterial inactivation in SMWWTPE at circumneutral pH by direct solar disinfection as a function of UV irradiance versus time (A) and dose (B). The arrow indicates the order in which the data series appear in the figure.

context of solar disinfection, it has been reported greater effectiveness of applying a higher intensity for a short time than a lower intensity for a longer period of time, indicating that the action of repair enzymes in the cell is favoured at lower UV intensities [34].

Direct solar disinfection is considered a complex process with multisteps acting simultaneously that result in the inactivation of the microorganisms. Induced by UVA light [35,36], internal reactive oxygen species (ROS) are produced inside the cell and it is the accumulation of ROS attacks what leads to bacterial death [37]. Additionally, the photoinactivation of two essential enzymes of the defence system against intracellular oxidative stress takes place. The role of these enzymes is acting as scavenger of ROS against the photo-oxidative damage: catalase (CAT) for hydrogen peroxide, and superoxide dismutase (SOD) for superoxide radicals [24]. It is accepted that UV-B causes damages in DNA by direct absorption of light by endogenous chromophores [38]. Temperature also affects the solar disinfection process inducing a synergetic effect with sunlight that shortens the treatment time with

increased temperature values [8], but strongly when temperatures are above 45 °C [39].

Taking into account the mechanistic features mentioned above, our approach for the kinetic modelling of the direct solar inactivation of microorganisms was based on the consideration of a minimum photonic energy needed to reach a lethal effect through a sequence of reversible damage that can be reverted by the cell repairing mechanisms. Therefore, low irradiance level can damage the cell, but not enough to overcome self-repair mechanism. The proposed model, based on the threshold or multi-hit concept of the *serial n-event* model, considers that the effect of radiation is a process of accumulation of hits or reversible structural damages in the cell and that inactivation occurs when n unrepaired hits have accumulated. A model with 3 kinetic parameters is proposed, in which the inactivation of undamaged bacteria (B_u) takes place through a reversible sequence of damaged steps ($B_{d,i}$) until eventually become inactivated (B_{inact}) corresponding to the n level of damage ($B_{d,n}$):

$$B_u \underset{k_{solar,repair}}{\overset{k_{solar}}{\rightleftarrows}} B_{d,1} \underset{k_{solar,repair}}{\overset{k_{solar}}{\rightleftarrows}} B_{d,2} \underset{k_{solar,repair}}{\overset{k_{solar}}{\rightleftarrows}} \cdots B_{d,i} \cdots \underset{k_{solar,repair}}{\overset{k_{solar}}{\rightleftarrows}} B_{d,n-2} \underset{k_{solar,repair}}{\overset{k_{solar}}{\rightleftarrows}} B_{d,n-1} \overset{k_{solar}}{\rightarrow} B_{inact}$$

where k_{solar} is the rate constant of direct solar inactivation ($m^2\ J^{-1}$), k_{repair} is the first-order self-repairing constant (s^{-1}) and n is the threshold level of damage. Based on this scheme, the balance of the microorganism B at the event-level i can be expressed as:

$$\frac{d[B_{d,i}]}{dt} = k_{solar}[B_{d,i-1}] + k_{solar,repair}[B_{d,i+1}] - k_{solar}[B_{d,i}] - k_{solar,repair}[B_{d,i}] \quad (5)$$

The total concentration of surviving microorganisms is the sum of the concentration of all the microorganisms from B_u to $B_{d,n-1}$, corresponding to the last damage level before the inactivation threshold.

Fig. 4 shows the best fit of the experimental data, achieved for threshold value of $n = 5$. The values of the kinetic constants are shown in Table 1. The presence of the reversible repairing process combined with the concept of a threshold makes possible to predict the non-linear behaviour of the bacterial inactivation with respect to the irradiance, although the model slightly overestimates the bactericidal effect for 25 W m^{-2}. This low irradiance region of negligible inactivation is better adjusted with an $n = 6$ model, although with a higher global error due to the worse correlation for the experimental data at higher irradiance in which significant inactivation takes place.

The threshold number of attacks ($n = 5$) is lower than the value of 9 reported by Severin et al. [11] for UVC inactivation of *E. coli* disinfection. The reason is that our experimental data show almost negligible shoulders (the presence of a long shoulder is indicative of a higher number of threshold damages). On the other hand, the kinetic constant reported here is considerably lower, as expected for solar UV (UVA and UVB), in comparison with UV-C. Apart from the obvious differences in the UV-C *vs* solar UV inactivation mechanisms, this indicates that the quantum yield of the solar process is significantly lower (most of the absorbed photons are harmless).

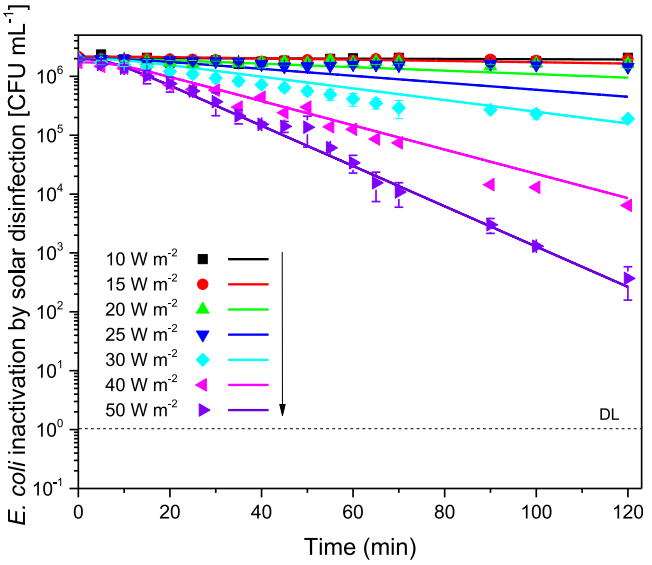

Fig. 4. Correlation between experimental data (dots) and model predictions (lines) with the *serial n-event* kinetic model for direct solar inactivation of *E. coli*. The arrow indicates the order in which the data series appear in the figure.

3.3. Modelling of the photo-Fenton inactivation of microorganisms

3.3.1. Hydrogen peroxide consumption

H_2O_2 concentration was monitored during the photo-Fenton experiments. Fig. S.2 shows the results of H_2O_2 consumption for increasing irradiance values and two initial concentration of iron of 10 and 20 mg L^{-1}. For low irradiances values the system operates under irradiance limitation, whereas for high irradiances the concentration of iron limits the process, and the system works under excess of radiation, reaching a photosaturation limit. These results are in agreement with previous studies [19]. Fig. 5 shows the first-order rate constant of hydrogen peroxide consumption calculated from the 0–40 min irradiation period (dark reduction of Fe^{3+} at this temperature was not significant). For the optical pathway of 5 cm used in the present work, the iron limitation is achieved above 20 and 25 W m^{-2} for 10 and 20 mg L^{-1} of iron, respectively. Above 25 W m^{-2}, the rate constant of hydrogen peroxide consumptions is essentially constant.

The photo-Fenton process at acidic conditions is usually represented by R1′ to R3′. The main reaction in Fenton process is the Haber Weiss R1′ reaction [1]:

$$Fe^2 + H_2O_2 \rightarrow Fe^{3+} + OH^- + HO \qquad (R1') \qquad (k_1' = 50 - 70\ Lmol^{-1}s^{-1})$$

Fe^{3+} reduction through R2′ also occurs, but the rate is considerably slower and is usually not considered [1]:

$$Fe^{3+} + H_2O_2 \rightarrow Fe^{2+} + HO_2 + H^+ \qquad (R2') \qquad (k_2' = 3.1 \times 10^{-3}\ Lmol^{-1}s^{-1})$$

The production of $HO^{\cdot}$ is greatly increased upon UV illumination by the photo-Fenton reaction R3′ that closes the iron catalytic cycle:

$$Fe^{3+} + H_2O \rightarrow Fe^{2+} + HO^{\cdot} + H^+ \qquad (R3')$$

Since Fe^{2+} is regenerated via R3′ with decomposition of water rather than H_2O_2 (R2′), the photo-Fenton process consumes less H_2O_2 and requires only catalytic amounts of Fe^{2+} [26].

Table 1
Serial n-event kinetic model proposed for direct solar inactivation of microorganisms.

Step	Reaction	Rate	Values for *E. coli*
Solar damage of microorganism	$B_u \xrightarrow{h\upsilon} B_{d,1}$	$k_{solar}\,[B_u]\,G$	$k_{solar} = 1.54 \times 10^{-4}\ m^2\ J^{-1}$ $n = 5$
	$B_{d,1} \xrightarrow{h\upsilon} B_{d,2}$	$k_{solar}\,[B_{d,1}]\,G$	
	$B_{d,i} \xrightarrow{h\upsilon} B_{d,i+1}$	$k_{solar}\,[B_{d,i}]\,G$	
	$B_{d,n-1} \xrightarrow{h\upsilon} B_{inact}$	$k_{solar}\,[B_{d,n-1}]\,G$	
Microorganism self-repair	$B_{d,1} \rightarrow B_u$	$k_{solar,repair}\,[B_{d,1}]$	$k_{solar,repair} = 4.79 \times 10^{-3}\ s^{-1}$
	$B_{d,2} \rightarrow B_{d,1}$	$k_{solar,repair}\,[B_{d,2}]$	
	$B_{d,i} \rightarrow B_{d,i-1}$	$k_{solar,repair}\,[B_{d,i}]$	
	$B_{d,n-1} \rightarrow B_{d,n-2}$	$k_{solar,repair}\,[B_{d,n-1}]$	

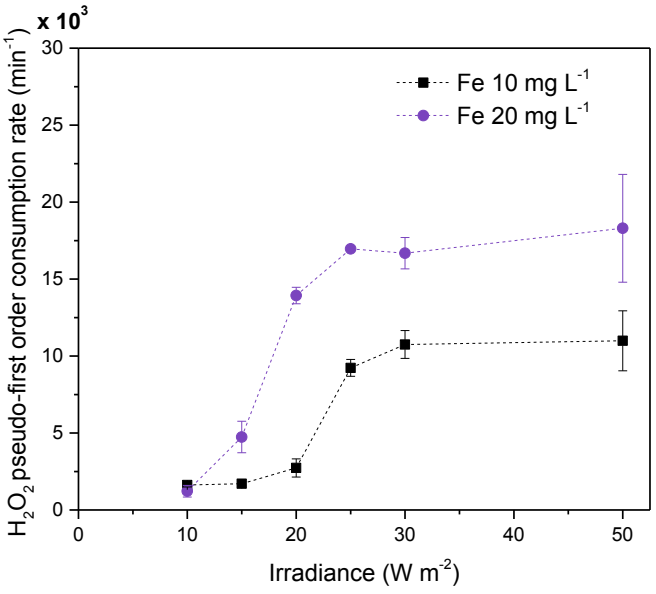

Fig. 5. First-order rate constants of hydrogen peroxide consumption as a function of iron concentration and irradiance.

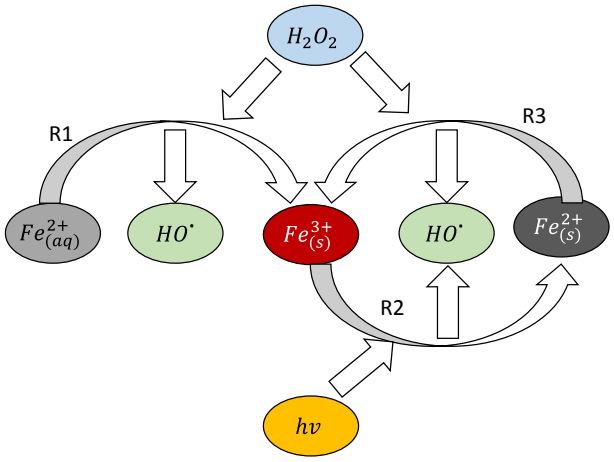

Fig. 6. Schematic representation of the proposed mechanism for the photo-Fenton process at circumneutral pH.

Modelling of the photo-Fenton process at circumneutral pH including the existence of a photosaturation region, requires the elucidation of the role of the precipitated iron species. Our approach considers that the photo-Fenton process is mediated by the iron species in the heterogeneous solid phase, as represented in Fig. 6. After the initial R1′ reaction (transformed now to R1 to consider the precipitation of the oxidized Fe^{3+}, due to the negligible concentration of soluble Fe^{3+} species, both R2′ and R3′ can be neglected. The process in then controlled by the equivalent heterogeneous processes to R1′ and R3′, that would be R3 and R2, respectively.

Table 2 summarizes the proposed reactions for the photo-Fenton process. In the first Fenton reaction (R1) it is assumed that the aqueous iron precipitates as iron hydroxides at neutral pH. This process only takes place in the initial stages of the process when fresh Fe^{2+} is supplied to the reaction bulk. Once the $Fe^{2+}_{(aq)}$ is consumed, $Fe^{3+}_{(s)}$ can be photoreduced to $Fe^{2+}_{(s)}$, both in the solid phase by R2. $Fe^{2+}_{(s)}$ can be re-oxidized to $Fe^{3+}_{(s)}$ by hydrogen peroxide. When R3 controls the global process, photosaturation occurs. As the concentration of iron is higher working at 20 mg L^{-1}, a higher absorption of photons takes place and, consequently, a higher hydrogen peroxide decomposition rate is expected, as long as irradiance is the limiting factor. Then, the photoreduction reaction of Fe^{3+} becomes faster and the reaction rate is controlled by oxidation of precipitated Fe^{2+} by hydrogen peroxide. This last reaction is independent of light intensity, leading to the photosaturation effect.

The resolution of mass balances of the different species assuming the kinetic micro steady-state for the hydroxyl radical leads to the calculation of the concentration of the 3 iron species, $Fe^{2+}_{(aq)}$, $Fe^{3+}_{(s)}$ and $Fe^{2+}_{(s)}$ and H_2O_2 concentration. The derivation of the kinetic model is detailed in Appendix A. A first fitting of the experimental data of H_2O_2 consumption was carried out independently on the bacterial inactivation. This simple model is proved to be accurate enough for representing the experimental photosaturation effect as well as the photolimited region at low irradiance, successfully fitting the experimental results with a NMRSE of 8.51% (Fig. 7). Saturation effect is satisfactorily reproduced for a concentration of iron of 10 mg L^{-1}, although for 20 mg L^{-1} of Fe the model predicts the saturation effect for 30 W m^{-2} whilst the experimental data reveals this effect at 20 W m^{-2}. Globally, we consider that the model is a good compromise between a very complex rigorous mechanistic approach considering all possible reactions taking place in the system and a simplified empiric approach, providing acceptable predictive modelling of the photo-Fenton process at circumneutral conditions.

The value obtained for k_1 of 19.95 M s^{-1} is in the order of the classical values reported in the literature for k_1' at acidic conditions, between 50 and 70 M^{-1} s^{-1} [31,32]. Fenton rate for precipitate Fe^{2+} species is slower than the soluble phase, as expected. Predicted $Fe^{2+}_{(s)}$ and $Fe^{3+}_{(s)}$ by the kinetic model used in this research are presented in Fig. 8. $Fe^{2+}_{(aq)}$ is quickly consumed during the first minutes by reaction R1, forming $Fe^{3+}_{(s)}$. The difference between the initial total iron that remains constant, and the sum of the two solid species corresponds to $Fe^{2+}_{(aq)}$.

Table 2
Reactions included in the direct solar inactivation model and obtained parameters values.

Reaction	Rate	Kinetic constant	Units
R1) $Fe^{2+}_{(aq)} + H_2O_2 \rightarrow Fe^{3+}_{(s)} + HO$	$k_1\ [Fe^{2+}_{(aq)}]\ [H_2O_2]$	$k_1 = 19.95$	$M^{-1}\ s^{-1}$
R2) $Fe^{3+}_{(s)} + H_2O \xrightarrow{h\upsilon} Fe^{2+}_{(s)} + HO\cdot + H^+$	$k_2'\ [H_2O]\ G\ [Fe^{3+}_{(s)}] \approx k_2\ G\ [Fe^{3+}_{(s)}]$	$k_2 = 3.92 \times 10^{-5}$	$m^2\ J^{-1}$
R3) $Fe^{2+}_{(s)} + H_2O_2 \rightarrow Fe^{3+}_{(s)} + HO^{\cdot} + H^+$	$k_3\ [Fe^{2+}_{(s)}]\ [H_2O_2]$	$k_3 = 7.66$	$M^{-1}\ s^{-1}$

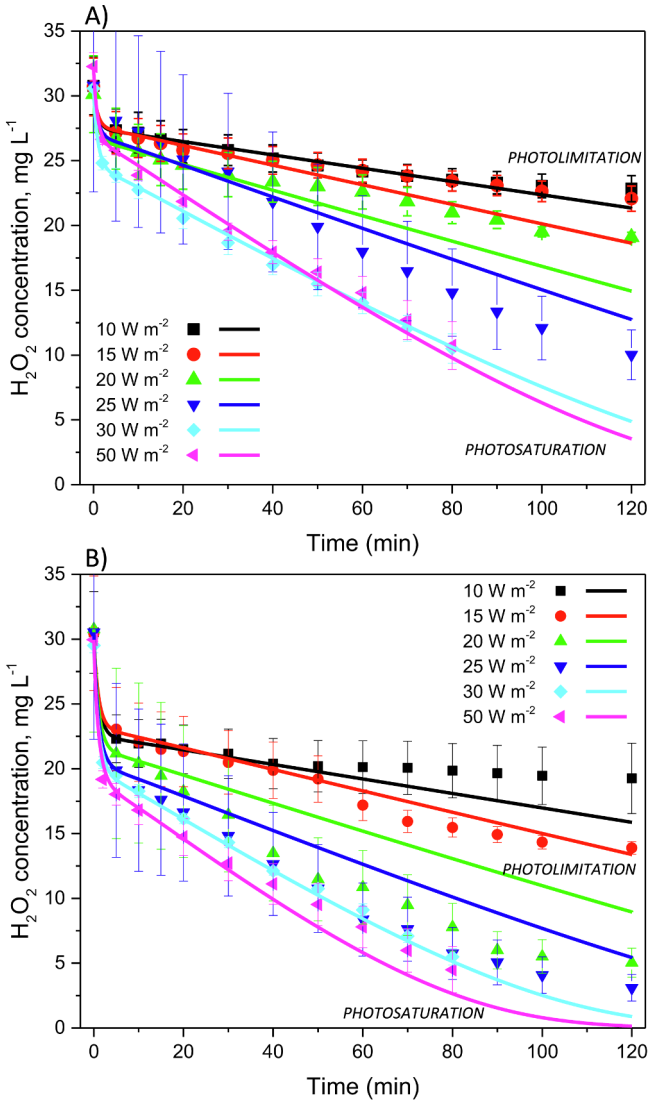

Fig. 7. Correlation between experimental data (dots) and model predictions (lines) for H_2O_2 consumption during photo-Fenton process at circumneutral pH with A) 10 and B) 20 mg L^{-1} of Fe.

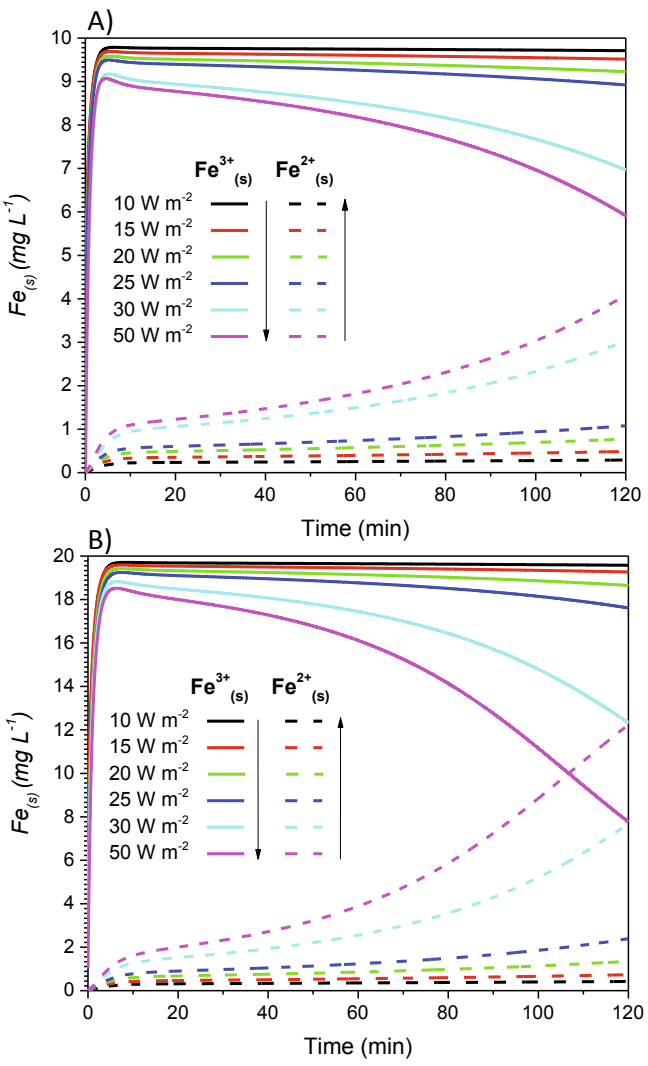

Fig. 8. Model results for Fe oxidation state distribution during photo-Fenton reactions at circumneutral pH. A) For an initial Fe concentration of 10 mg L^{-1} B) For 20 mg L^{-1} of Fe. The arrow indicates the order in which the data series appear in the figure.

In the cases where the system works under photolimitation conditions (up to 25 W m^{-2}), the predominant oxidation state is $Fe^{3+}_{(s)}$ because the rate-limiting step is the photoreduction of $Fe^{3+}_{(s)}$ to $Fe^{2+}_{(s)}$ (reaction R2 in Table 2). This also occurs during the first hour of reaction in experiments at 30 and 50 W m^{-2}, but as H_2O_2 is consumed, the oxidation reaction from $Fe^{2+}_{(s)}$ to $Fe^{3+}_{(s)}$ slows down (reaction R3 in Table 2), approaching an equilibrium that corresponds to the photosaturation region.

3.3.2. Bacterial inactivation

Results of the photo-Fenton inactivation of *E. coli* at circumneutral pH are shown in Fig. 9. For the higher irradiance values, both iron concentrations lead to a 6-log decay within 60 min of illumination. Negligible *E. coli* inactivation is observed for the lowest irradiance of 10 W m^{-2}, and a relatively low inactivation level in the range 15 to 20 W m^{-2} what can be attributed to a low generation of hydroxyl radicals in comparison with the efficiency of the self-repairing bacterial processes. It can be observed that despite the photosaturation effect observed in the consumption of H_2O_2, the bacterial inactivation is

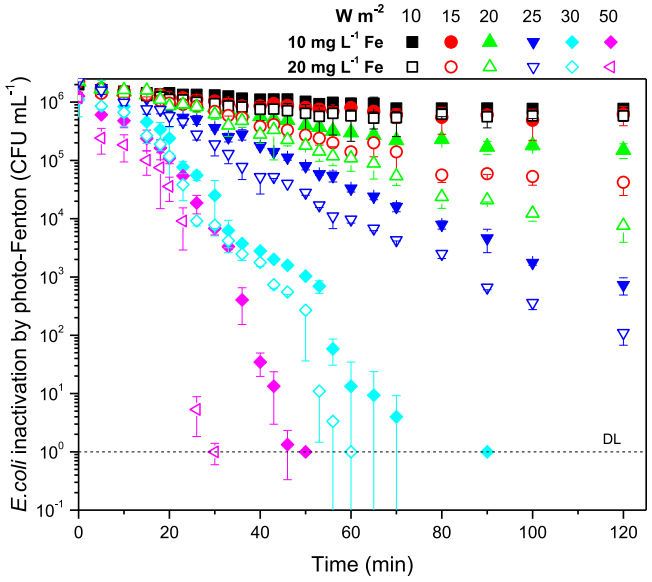

Fig. 9. Experimental results of *E. coli* inactivation with the photo-Fenton process at circumneutral pH, for initial iron concentrations of 10 and 20 mg L^{-1}, and irradiance values between 10 and 50 W m^{-2}.

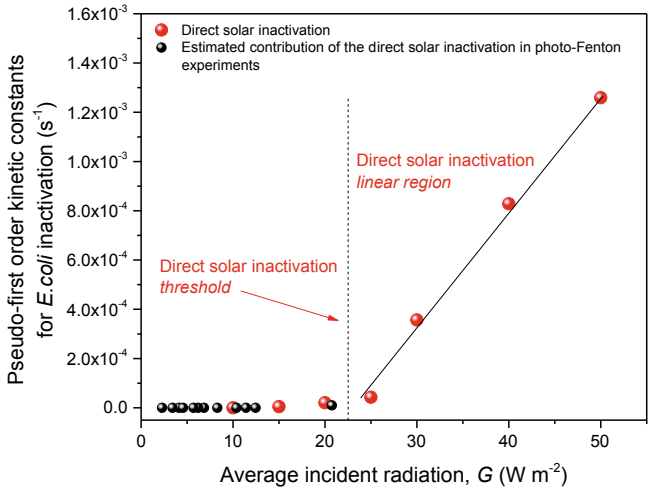

Fig. 10. Comparison of the disinfection rates calculated for the direct solar disinfection process and the estimated contribution of the process during the photo-Fenton experiments as a function of the average incident radiation considering the absorption of photons by the iron species.

significantly improved for 50 W m^{-2} in comparison with 30 W m^{-2}.

In comparison with the direct solar inactivation, the photo-Fenton process provides a significantly higher disinfection efficiency, leading to a 6-log inactivation in 50 min for 10 mg L^{-1} of iron (30 min for 20 mg L^{-1}), while only 3-log decay was obtained after 120 min of the direct solar process, in all cases for 50 W m^{-2} of irradiance. The reason is that in addition to the direct photonic damages, the photo-Fenton process proceeds simultaneously through the hydroxyl radicals' inactivation route. In fact, the effect of direct solar inactivation is expected to be low in the global photo-Fenton disinfection process, since the radiation absorbed by iron is quite high and there is not much light available for the direct absorption of photons by the bacteria. Fig. 10 shows how the values of the disinfection rates predicted by the direct solar inactivation model are below the observed threshold level.

It has been previously reported that bacterial inactivation is significantly higher when the cells are exposed to different stress sources [40]. In photo-Fenton processes, two different stress sources have to be considered: HO˙ oxidation of the bacteria vital constituents, and direct photonic effect. Therefore, even if the theoretical contribution of the direct solar inactivation could seem negligible (Fig. 10), the potential synergy between both processes have to be considered. To develop a mechanistic modelling approach of the process, some aspects must be considered to get consistency whether both agents are simultaneously present or not:

- To allow reversibility and synergy, single hit models cannot be considered, as the bacteria need the first attack to activate defence mechanisms.
- The kinetic constant for the attack by each individual mechanism should keep its value in both single-stress and multiple-stress scenarios, because elementary kinetic constant value could depend on the chance of a clash, the required energy, steric effects, etc., and none of this should be affected by the other stressing agent.
- The number of serial attacks required by a single agent to inactivate a bacterium must remain constant if the bacterium does not receive any attack from the other agent.

On the one hand, radiation and radicals may be attacking the same target in the bacteria, and their effects should stack. In this *single target – multiple hit* scenario, there would be several levels, with both effects going forward at the same or different rates. A single repairing constant would be considered, being impossible to determine at a given level if the bacteria reached this point through one type of attack or the other. The synergy comes from the possibility of replacing attacks from one source by attacks from the other. On the other hand, each agent may be attacking a different target in the bacteria. In this *multiple target – multiple hit* scenario, each bacterium keeps a record of the number of attacks of each type, building a matrix of two dimensions, one per stress agent. The attack of an agent moves the bacteria one step forward in its dimension, while there are independent regenerations, moving the bacteria one step back. There are two new regeneration constants, with lower values, for bacteria that have already received both types of attacks. This decrease in regeneration rate is the synergistic effect. Both models were studied and used for fitting the experimental data but the *multiple target – multiple hit* model was the only one provided meaningful results.

Based on the preliminary results from the direct solar inactivation process, it was possible to quantify that 5 levels of photonic attack need to be considered to reach the bacterial inactivation. Therefore, this was the level of damage considered for the photonic effect on the photo-Fenton matrix. In the case of the absence of the hydroxyl radical mechanism (absence of iron and H_2O_2) the values of the kinetic parameters would be those previously reported (n, k_{solar}, $k_{solar,repair}$). On the contrary, in the presence of the HO˙ inactivation route, the kinetic constant of the self-repairing process for from a combined damage would be lower ($k_{solar,repair2}$) to account for the synergy between both inactivation mechanisms. Similarly, the bacteria could be inactivated after a threshold level of HO˙ damages (k_{HO}) and could be recovered also from the intermediate levels of damage ($k_{HO,repair}$) but will do it less effectively from combined damages states ($k_{HO,repair2}$). Fig. 11 schematizes the proposed mechanism for the *multiple target – multiple hit* kinetic model.

The total concentration of surviving organisms can be calculated as the sum of all organisms below the threshold damage levels, i.e., over the last row, before the last column.

In addition to the bacterial inactivation process, the high reactivity and non-selectivity of HO˙ towards both organic and inorganic

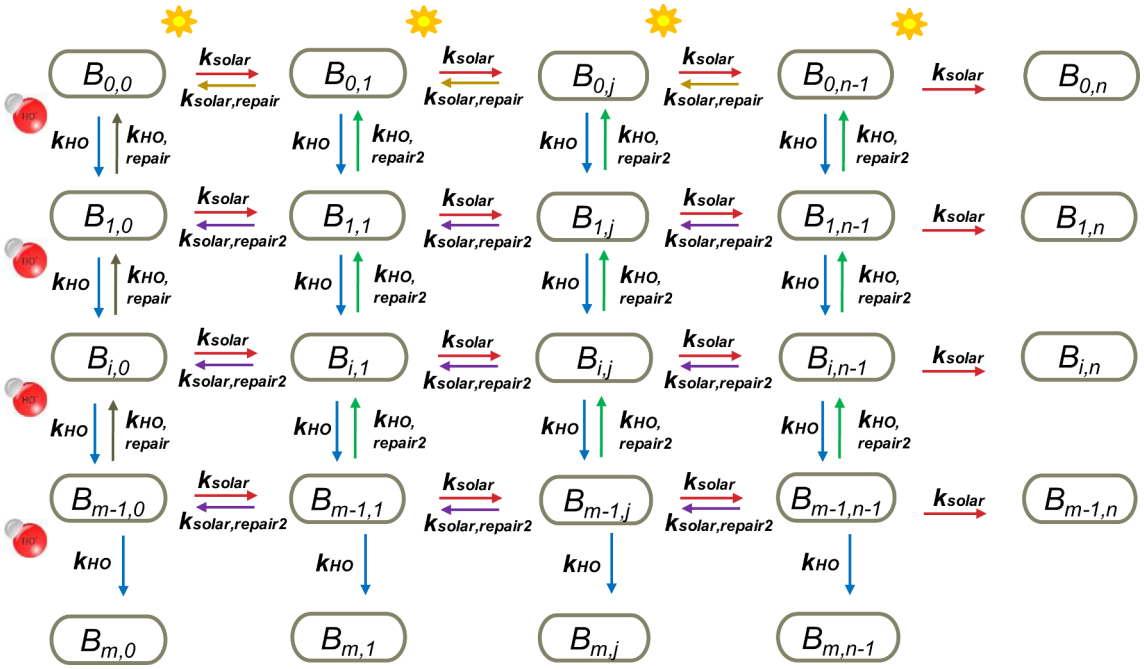

Fig. 11. Schematic representation of the proposed *multiple target – multiple hit* kinetic model for the inactivation of bacteria by the photo-Fenton process.

Table 3
Additional reactions included in photo-Fenton disinfection model and values of the kinetic parameters (see Tables 1 and 2 for the direct solar inactivation and Fenton reactions).

Reaction	Rate	Value		Units
R4) $HO^{\cdot} + HO^{\cdot} \rightarrow H_2O_2$	$k_4\ [HO^{\cdot}]^2$	3.98×10^9		$M^{-1}\ s^{-1}$
R5) $OM_{RED} + HO^{\cdot} \rightarrow OM_{OX}$	$k_5'\ [OM_{RED}]\ [HO^{\cdot}] \approx k_5\ [HO^{\cdot}]$	1.12×10^5		s^{-1}
R6) $B_{i,\,j} + HO^{\cdot} \rightarrow B_{i+1,\,j}$	$k_{HO}\ [B_{i,\,j}]\ [HO^{\cdot}]$	8.98×10^9	$m = 27$	$M^{-1}\ s^{-1}$
R7) $B_{i,0} \rightarrow B_{i-1,0}$	$k_{HO,repair}\ [B_{i,0}]$	6.26×10^{-3}		s^{-1}
R8) $B_{i,\,j\neq 0} \rightarrow B_{i-1,j\neq 0}$	$k_{HO,repair2}\ [B_{i,\,j\neq 0}]$	3.16×10^{-8}		s^{-1}
R9) $B_{i\neq 0,\,j} \rightarrow B_{i\neq 0,j-1}$	$k_{solar,repair2}\ [B_{i\neq 0,\,j}]$	1.31×10^{-4}		s^{-1}

substrates ($k > 10^8\ M^{-1}s^{-1}$ [41]) results in various competitive processes that negatively affect the global oxidation process [42]. Therefore, these competitive processes have to be considered also for the accurate calculation of the concentration of hydroxyl radicals available for the disinfection process. Moreover, in the presence of carbonates, the $CO^{3-\cdot}$ radical can play an important role in the consumption of $HO^{\cdot}$ radicals [43]. In the present model, for the sake of simplicity, the scavenging of $HO^{\cdot}$ radicals by organic and inorganic substances has been included in the same reaction. Table 3 summarizes the additional reactions included in the final model, together with the direct solar inactivation and Fenton reactions shown in Tables 1 and 2, respectively. The concentration of the $HO^{\cdot}$ radical was calculated assuming kinetic micro steady-state approximation.

Summarising, model regression was carried out in three steps:

- The experimental data for *E. coli* inactivation by direct solar disinfection were fitted first to the proposed solar inactivation kinetic model, being calculated the values of n, k_{solar} and $k_{solar,repair}$.
- The experimental data for H_2O_2 consumption during photo-Fenton inactivation were then fitted to the photo-Fenton reactions R1 to R3, being calculated the values of k_1, k_2 and k_3.
- The global model for photo-Fenton process is finally fitted using as error function a weighted sum between the NRMSLE of bacterial inactivation and the NRMSE of H_2O_2 consumption. Previously calculated parameters were used as seed values for this final fitting in which the concentration of $HO^{\cdot}$ also takes into account the radical consumption reactions in Table 3.

Fig. 12 shows how the model successfully predicts the experimental data of bacterial inactivation with a low NMRLSE value of 2.74%. The values calculated for the kinetic parameters of the photo-Fenton model are shown in Table 3. As expected, the self-repairing constants from combined damages levels are lower than those from the individual mechanisms ($k_{solar,repair2} = 1.31 \times 10^{-4}\ s^{-1}$ *vs* $k_{solar,repair} = 4.79 \times 10^{-3}\ s^{-1}$, and $k_{HO,repair2} = 3.16 \times 10^{-8}\ s^{-1}$ *vs* $k_{HO,repair} = 6.26 \times 10^{-3}$). As previously discussed [44], the high value of the kinetic constants involving the $HO^{\cdot}$ radicals suggests that they are reaction limited by diffusion, with almost null activation energies, and no dependence on temperature. This fact, combined with the short life of a hydroxyl radical, raises the importance of the proper reactor design to ensure optimal mixing and contact between radical sources and bacteria.

The estimated threshold number of $HO^{\cdot}$ attacks ($m = 27$) is 5.5 times higher than the threshold number of damages by the direct

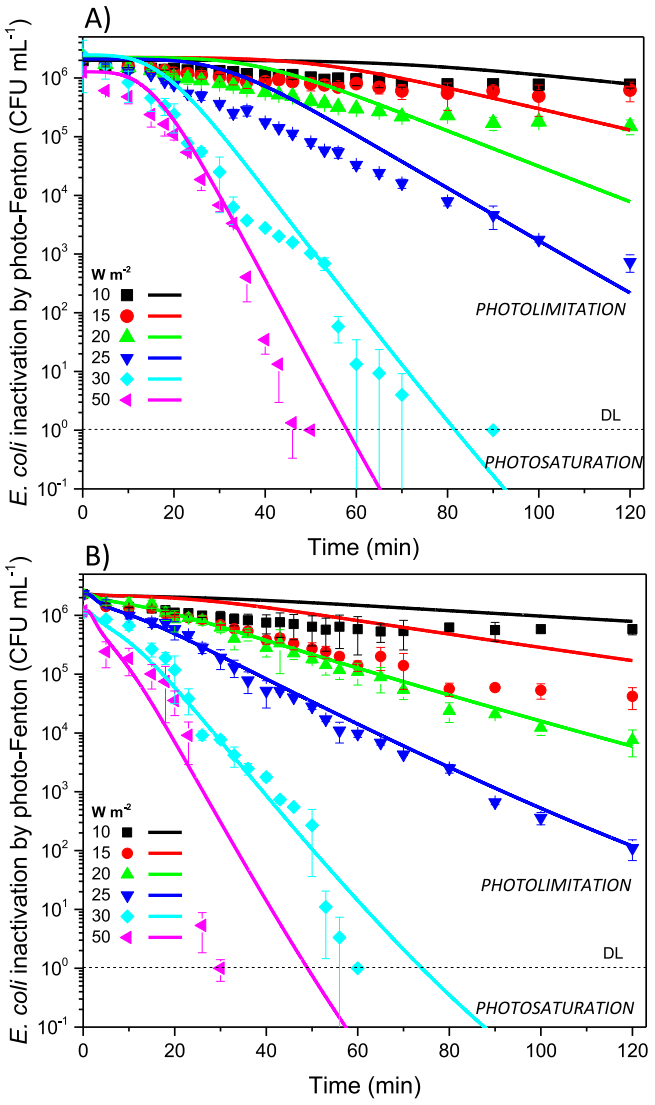

Fig. 12. Correlation between experimental data (dots) and model predictions (lines) for the bacterial inactivation with photo-Fenton process at circumneutral pH for UV irradiance values between 10 and 50 W m^{-2} and iron concentrations of A) 10 and B) 20 mg L^{-1}.

photonic process, giving a reasonable comparison between the potential damage produced by radicals or photons. Moreover, the synergistic constant for self-repairing of radical damages is much lower than the solar one, and it must also go through a higher number of levels to completely heal the bacteria. This is the reason for the pronounced curvature of the curves in Fig. 12**A**, where the available radiation after iron absorption is higher. With no regeneration to straighten the curves, the effect of series events prevails.

4. Conclusions

The proposed *multiple target – multiple hit* kinetic modelling has been proved to be a successful approach for photo-Fenton disinfection processes. This model represents a suitable compromise between a simplified engineering description and the impractical attempt to describe rigorously the very complex microbiological and chemical processes involved in the inactivation of the microorganisms. The application of the model has been successfully validated with experimental data on inactivation of *E. coli* bacteria at circumneutral pH. Both mechanisms of photonic direct solar inactivation and hydroxyl radicals based oxidation are properly described both individually and in their synergistic combination.

For the direct solar inactivation, the non-linear dependence of bacterial inactivation with dose has been successfully described by a *serial n-event* kinetic model in which the required inactivation threshold is achieved through 5 reversible events of incremental damages than can be reverted by the self-repairing mechanism of the cells. This model can explain why the use of irradiance values below 20 W m^{-2} led to almost negligible inactivation results for *E. coli* at circumneutral pH.

Regarding the Fenton-based process, a modification of the classical homogeneous reaction scheme has been proved to be capable of reproducing the H_2O_2 consumption in the heterogeneous process that takes place at circumneutral pH, including the limiting conditions of photolimitation and photosaturation. These limiting situations have been successfully predicted based on the radiation transport in the reactor, for which the optical properties of the precipitated iron hydroxides suspensions have been calculated and the VRPA estimated.

Future studies should focus on the challenging integration in the model of the effect of temperature and water composition, as the kinetic parameters reported here are limited to the specific conditions used for the experimental data. In any case, the developed model contributes significantly to the mechanistic understanding of the process and can be easily extrapolated to other indicator microorganisms or operational conditions just recalculating the values of the rate constants.

Declaration of Competing Interest

The authors declare that they have no known competing financial interests or personal relationships that could have appeared to influence the work reported in this paper.

Acknowledgements

The authors gratefully acknowledge the financial support of the European Union's Horizon 2020 research and innovation programme in the frame of the PANIWATER project (GA 820718), the Comunidad de Madrid and European Structural Funds [FOTOCAOS project, Y2018/EMT-5062] and the LIFE ULISES project funded by the European Union under the LIFE Financial Programme Grant Agreement No. LIFE18 ENV/ES/000165.

Appendix A

Derivation of the kinetic model

The kinetic model proposed for the photo-Fenton disinfection is based on the reaction schemes summarized in Tables 1–3. The concentration of total iron is constant during the experiments, and $Fe^{3+}_{(s)}$ concentration is calculated from the balance between the initial concentration of iron and the concentration of the reduced species:

$$[Fe^{3+}_{(S)}] = [Fe] - [Fe^{2+}_{(s)}] - [Fe^{2+}_{(aq)}] \quad \text{(A1)}$$

The concentration of the rest of iron species and hydrogen peroxide are calculated using Euler explicit method with a time step of 0.1 s (optimized after a preliminary independence study) using the time derivatives of each compound:

$$\frac{d[Fe^{2+}_{(aq)}]}{dt} = -k_1[Fe^{2+}_{(aq)}][H_2O_2] \tag{A2}$$

$$\frac{d[Fe^{2+}_{(s)}]}{dt} = k_2 G[Fe^{3+}_{(s)}] - k_3[Fe^{2+}_{(s)}][H_2O_2] \tag{A3}$$

Where the concentration of water has been assumed constants and included in the value of the kinetic constant $k_2 = k_2'[H_2O]$
Introducing Eq. (A1) in Eq. (A3):

$$\frac{d[Fe^{2+}_{(s)}]}{dt} = k_2 G([Fe] - [Fe^{2+}_{(s)}] - [Fe^{2+}_{(aq)}]) - k_3[Fe^{2+}_{(s)}][H_2O_2] \tag{A4}$$

The reaction rate of H_2O_2 is expressed as:

$$\frac{d[H_2O_2\ ]}{dt} = -k_1[Fe^{2+}_{(aq)}][H_2O_2] - k_3[Fe^{2+}_{(s)}][H_2O_2] \tag{A5}$$

By applying the kinetic micro steady-state approximation (MSSA) for the concentration of HO$^{\cdot}$, the following expression can be derived:

$$\frac{d[HO\cdot]}{dt} = k_1[Fe^{2+}_{(aq)}][H_2O_2] + k_2 G[Fe^{3+}_{(s)}] + k_3[Fe^{2+}_{(s)}][H_2O_2] - 2k_4[HO\cdot]^2 - k_5[HO\cdot] - \Sigma k_{HO}[Bi,j][HO\cdot] \approx 0 \tag{A6}$$

Both the kinetic constant k_{HO} and the HO$^{\cdot}$ concentration can be taken out of the summation in Eq. (A6). Grouping terms and solving the resulting quadratic equation, the concentration of hydroxyl radicals takes the following expression:

$$[HO\cdot] = \frac{k_5 + k_{HO}\sum[Bi,j] - \sqrt{(k_5 + k_{HO}\sum[Bi,j])^2 + 8\ k_4(k_1\ [Fe^{2+}_{(aq)}][H_2O_2] + \ k_2 G[Fe^{3+}_{(s)}] + k_3[Fe^{2+}_{(s)}][H_2O_2])}}{-4k_4} \tag{A7}$$

The concentration of the organic matter and other possible scavenger species was considered constant and included in the value of the kinetic constant $k_5 = k_5'[OM_{RED}]$.

The concentration of all levels of bacterial damage considering both stress sources are tracked using a 2D matrix. All the values of the matrix are initialized at zero, except the undamaged bacteria $B_{0,0}$, where the initial concentration is set. Each position is then calculated using the Euler explicit method with the same time step of 0.1 s using Eq. (A8):

$$\frac{d[B_{i,j}]}{dt} = k_{HO}[B_{i-1,j}][HO\cdot] + k_{Solar}G[B_{i,j-1}] + k_{HO,repair}[B_{i+1,j}] + k_{Solar,repair}[B_{1,j+1}] - (k_{HO}[HO\cdot] + k_{Solar}G + k_{HO,repair} + k_{Solar,repair})[B_{i,j}] \tag{A8}$$

The first two terms on the right-hand side of Eq. (A8) represent the increase in the concentration of bacteria at a given level of damage due to attacks to bacteria at the previous levels of damage by HO$^{\cdot}$ and photons, respectively. Therefore, the first term is not present in the balance of bacteria that have not received any HO$^{\cdot}$ attack yet ($i = 0$). The same applies to the second term in bacteria levels with no solar attacks ($j = 0$). None of these two terms are present in the balance of undamaged bacteria.

Similarly, the third and fourth terms on the right-hand side of Eq. (A8) represent the bacteria repaired from levels above the current one. The third term is not present in the balance of bacteria in the last column of the matrix ($i = m\text{-}1$), because bacteria with m HO$^{\cdot}$ attacks are already inactivated. The same happens to the fourth term in the last row ($j = n\text{-}1$). Finally, the fifth term is the reduction of bacteria concentration at the current level due to attacks to the next one or repairing processes to the previous one. Bacteria with no damages of any specific stress agent lacks the repair term of this type of damage. Bacteria with both types of damage ($i \neq 0$ and $j \neq 0$) use the synergistic kinetic constant of the repairing processes.

The total concentration of viable bacteria, corresponding to the values that can be compared with the experimental data, is calculated by the summation of bacteria concentration in all matrix levels before inactivation.

Appendix B. Supplementary data

Supplementary data to this article can be found online at https://doi.org/10.1016/j.cej.2020.126335.

References

[1] J.J. Pignatello, E. Oliveros, A. MacKay, Advanced oxidation processes for organic contaminant destruction based on the fenton reaction and related chemistry, Crit. Rev. Environ. Sci. Technol. 36 (2006) 1–84, https://doi.org/10.1080/10643380500326564.

[2] C. Ruales-Lonfat, J.F. Barona, A. Sienkiewicz, M. Bensimon, J. Vélez-Colmenares, N. Benítez, C. Pulgarín, Iron oxides semiconductors are efficients for solar water disinfection: a comparison with photo-Fenton processes at neutral pH, Appl. Catal. B Environ. 166–167 (2015) 497–508, https://doi.org/10.1016/j.apcatb.2014.12.007.

[3] H. Chick, An investigation of the laws of disinfection, J. Hyg. (Lond) 8 (1908) 92–158, https://doi.org/10.1017/S0022172400006987.

[4] H.E. Watson, A note on the variation of the rate of disinfection with change in the concentration of the disinfectant, Epidemiol. Infect. 8 (1908) 536–542, https://doi.org/10.1017/S0022172400015928.

[5] H.O.M. Lw, Kinetics of chlorine disinfection in an ecosystem, ASCE J. Sanit. Eng. Div. 98 (1972) 183–194.

[6] J.L. Rennecker, B.J. Mariñas, J.H. Owens, E.W. Rice, Inactivation of Cryptosporidium parvum oocysts with ozone, Water Res. 33 (1999) 2481–2488, https://doi.org/10.1016/S0043-1354(99)00116-5.

[7] R.J.W. Lambert, M.D. Johnston, Disinfection kinetics: a new hypothesis and model for the tailing of log-survivor/time curves, J. Appl. Microbiol. 88 (2000) 907–913, https://doi.org/10.1046/j.1365-2672.2000.01060.x.

[8] J. Marugán, R. van Grieken, C. Sordo, C. Cruz, Kinetics of the photocatalytic disinfection of Escherichia coli suspensions, Appl. Catal. B Environ. 82 (2008) 27–36, https://doi.org/10.1016/j.apcatb.2008.01.002.

[9] I. Najm, An alternative interpretation of disinfection kinetics, J. Am. Water Works Assoc. 98 (2006) 93–101, https://doi.org/10.1002/j.1551-8833.2006.tb07781.x.

[10] M.G. Corradini, M.D. Normand, M. Peleg, Stochastic and deterministic model of microbial heat inactivation, J. Food Sci. 75 (2010) R59–R70, https://doi.org/10.1111/j.1750-3841.2009.01494.x.

[11] B.F. Severin, M.T. Suidan, R.S. Engelbrecht, Kinetic modeling of U.V. disinfection of water, Water Res. 17 (11) (1983) 1669–1678, https://doi.org/10.1016/0043-1354(83)90027-1.

[12] B.F. Severin, M.T. Suidan, R.S. Engelbrecht, Series-event kinetic model for chemical disinfection, J. Environ. Eng. 110 (1984) 430–439, https://doi.org/10.1061/(ASCE)0733-9372(1984)110:2(430).

[13] C.N. Haas, A mechanistic kinetic model for chlorine disinfection, Environ. Sci. Technol. 14 (1980) 339–340, https://doi.org/10.1021/es60163a012.

[14] S. Giannakis, M. Voumard, S. Rtimi, C. Pulgarin, Bacterial disinfection by the photo-

Fenton process: Extracellular oxidation or intracellular photo-catalysis? Appl. Catal. B Environ. 227 (2018) 285–295, https://doi.org/10.1016/J.APCATB.2018.01.044.
[15] E. Ortega-Gómez, M.M.B. Martín, B.E. García, J.A.S. Pérez, P.F. Ibáñez, Wastewater disinfection by neutral pH photo-Fenton: the role of solar radiation intensity, Appl. Catal. B Environ. 181 (2016) 1–6, https://doi.org/10.1016/J.APCATB.2015.06.059.
[16] D. Rubio, E. Nebot, J.F. Casanueva, C. Pulgarin, Comparative effect of simulated solar light, UV, UV/H2O2 and photo-Fenton treatment (UV–Vis/H2O2/Fe2+,3+) in the Escherichia coli inactivation in artificial seawater, Water Res. 47 (2013) 6367–6379, https://doi.org/10.1016/J.WATRES.2013.08.006.
[17] D. Spuhler, J. Andrés Rengifo-Herrera, C. Pulgarin, The effect of Fe2+, Fe3+, H2O2 and the photo-Fenton reagent at near neutral pH on the solar disinfection (SODIS) at low temperatures of water containing Escherichia coli K12, Appl. Catal. B Environ. 96 (2010) 126–141, https://doi.org/10.1016/J.APCATB.2010.02.010.
[18] M. Kohantorabi, S. Giannakis, M.R. Gholami, L. Feng, C. Pulgarin, A systematic investigation on the bactericidal transient species generated by photo-sensitization of natural organic matter (NOM) during solar and photo-Fenton disinfection of surface waters, Appl. Catal. B Environ. 244 (2019) 983–995, https://doi.org/10.1016/J.APCATB.2018.12.012.
[19] I. Carra, J.L. García Sánchez, J.L. Casas López, S. Malato, J.A. Sánchez Pérez, Phenomenological study and application of the combined influence of iron concentration and irradiance on the photo-Fenton process to remove micropollutants, Sci. Total Environ. 478 (2014) 123–132, https://doi.org/10.1016/j.scitotenv.2014.01.066.
[20] A. Moncayo-Lasso, J. Sanabria, C. Pulgarin, N. Benítez, E. Simultaneous, coli inactivation and NOM degradation in river water via photo-Fenton process at natural pH in solar CPC reactor. A new way for enhancing solar disinfection of natural water, Chemosphere 77 (2009) 296–300, https://doi.org/10.1016/j.chemosphere.2009.07.007.
[21] P. Soriano-Molina, J.L. García Sánchez, S. Malato, L.A. Pérez-Estrada, J.A. Sánchez Pérez, Effect of volumetric rate of photon absorption on the kinetics of micropollutant removal by solar photo-Fenton with Fe 3+ -EDDS at neutral pH, Chem. Eng. J. 331 (2018) 84–92, https://doi.org/10.1016/j.cej.2017.08.096.
[22] J. Marugán, R. van Grieken, A.E. Cassano, O.M. Alfano, Kinetic modelling of the photocatalytic inactivation of bacteria, Water Sci. Technol. 61 (2010) 1547–1553, https://doi.org/10.2166/wst.2010.057.
[23] M. Castro-Alférez, M.I. Polo-López, J. Marugán, P. Fernández-Ibáñez, Mechanistic modeling of UV and mild-heat synergistic effect on solar water disinfection, Chem. Eng. J. 316 (2017) 111–120, https://doi.org/10.1016/J.CEJ.2017.01.026.
[24] M. Castro-Alférez, M.I. Polo-López, J. Marugán, P. Fernández-Ibáñez, Mechanistic model of the Escherichia coli inactivation by solar disinfection based on the photogeneration of internal ROS and the photo-inactivation of enzymes: CAT and SOD, Chem. Eng. J. 318 (2017) 214–223, https://doi.org/10.1016/J.CEJ.2016.06.093.
[25] A. Cabrera Reina, L. Santos-Juanes Jordá, J.L. García Sánchez, J.L. Casas López, J.A. Sánchez Pérez, Modelling photo-Fenton process for organic matter mineralization, hydrogen peroxide consumption and dissolved oxygen evolution, Appl. Catal. B: Environmental 119–120 (2012) 132–138, https://doi.org/10.1016/j.apcatb.2012.02.021.
[26] G. Rivas, I. Carra, J.L. García Sánchez, J.L. Casas López, S. Malato, J.A. Sánchez Pérez, Modelling of the operation of raceway pond reactors for micropollutant removal by solar photo-Fenton as a function of photon absorption, Appl. Catal. B Environ. 178 (2015) 210–217, https://doi.org/10.1016/j.apcatb.2014.09.015.
[27] P. Soriano-Molina, J.L. García Sánchez, O.M. Alfano, L.O. Conte, S. Malato, J.A. Sánchez Pérez, Mechanistic modeling of solar photo-Fenton process with Fe^{3+}-EDDS at neutral pH, Appl. Catal. B Environ. 233 (2018) 234–242, https://doi.org/10.1016/j.apcatb.2018.04.005.
[28] I. García-Fernández, M.I. Polo-López, I. Oller, P. Fernández-Ibáñez, Bacteria and fungi inactivation using Fe3+/sunlight, H2O2/sunlight and near neutral photo-Fenton: a comparative study, Appl. Catal. B Environ. 121–122 (2012) 20–29, https://doi.org/10.1016/J.APCATB.2012.03.012.
[29] M.I. Cabrera, O.M. Alfano, A.E. Cassano, Absorption and scattering coefficients of titanium dioxide particulate suspensions in water, J. Phys. Chem. 100 (1996) 20043–20050, https://doi.org/10.1021/jp962095q.
[30] J. Marugán, R. Van Grieken, O.M. Alfano, A.E. Cassano, Optical and physicochemical properties of silica-supported TiO2 photocatalysts, AIChE J. 52 (2006) 2832–2843, https://doi.org/10.1002/aic.10886.
[31] E. Ortega-Gómez, B. Esteban García, M.M. Ballesteros Martín, P. Fernández Ibáñez, J.A. Sánchez Pérez, Inactivation of natural enteric bacteria in real municipal wastewater by solar photo-Fenton at neutral pH, Water Res. 63 (2014) 316–324, https://doi.org/10.1016/j.watres.2014.05.034.
[32] B. Esteban García, G. Rivas, S. Arzate, J.A. Sánchez Pérez, Wild bacteria inactivation in WWTP secondary effluents by solar photo-fenton at neutral pH in raceway pond reactors, Catal. Today. 313 (2018) 72–78, https://doi.org/10.1016/j.cattod.2017.10.031.
[33] E. Ubomba-Jaswa, C. Navntoft, M.I. Polo-López, P. Fernandez-Ibáñez, K.G. McGuigan, Solar disinfection of drinking water (SODIS): an investigation of the effect of UV-A dose on inactivation efficiency, Photochem. Photobiol. Sci. 8 (2009) 587–595, https://doi.org/10.1039/b816593a.
[34] B. Sommer, A. Mariño, Y. Solarte, M.L. Salas, C. Dierolf, C. Valiente, D. Mora, R. Rechsteiner, P. Setter, W. Wirojanagud, H. Ajarmeh, A. Al-Hassan, M. Wegelin, SODIS – an emerging water treatment process, J. Water Supply Res. Technol. – AQUA 46 (1997) 127–137.
[35] R.M. Tyrrell, S.M. Keyse, New trends in photobiology the interaction of UVA radiation with cultured cells, J. Photochem. Photobiol. B Biol. 4 (1990) 349–361, https://doi.org/10.1016/1011-1344(90)85014-N.
[36] A.L. Santos, V. Oliveira, I. Baptista, I. Henriques, N.C.M. Gomes, A. Almeida, A. Correia, Â. Cunha, Wavelength dependence of biological damage induced by UV radiation on bacteria, Arch. Microbiol. 195 (2013) 63–74, https://doi.org/10.1007/s00203-012-0847-5.
[37] J. Marugán, R. van Grieken, C. Pablos, M.L. Satuf, A.E. Cassano, O.M. Alfano, Rigorous kinetic modelling with explicit radiation absorption effects of the photocatalytic inactivation of bacteria in water using suspended titanium dioxide, Appl. Catal. B Environ. 102 (2011) 404–416, https://doi.org/10.1016/j.apcatb.2010.12.012.
[38] K.G. McGuigan, R.M. Conroy, H.J. Mosler, M. du Preez, E. Ubomba-Jaswa, P. Fernandez-Ibañez, Solar water disinfection (SODIS): a review from bench-top to roof-top, J. Hazard. Mater. 235–236 (2012) 29–46, https://doi.org/10.1016/j.jhazmat.2012.07.053.
[39] P.M. Oates, P. Shanahan, M.F. Polz, Solar disinfection (SODIS): simulation of solar radiation for global assessment and application for point-of-use water treatment in Haiti, 2003.
[40] K.G. McGuigan, T.M. Joyce, R.M. Conroy, J.B. Gillespie, M. Elmore-Meegan, Solar disinfection of drinking water contained in transparent plastic bottles: characterizing the bacterial inactivation process, J. Appl. Microbiol. 84 (1998) 1138–1148, https://doi.org/10.1046/j.1365-2672.1998.00455.x.
[41] G.V. Buxton, C.L. Greenstock, W.P. Helman, A.B. Ross, Critical review of rate constants for reactions of hydrated electrons, hydrogen atoms and hydroxyl radicals (·OH/·O − in Aqueous Solution, J. Phys. Chem. Ref. Data 17 (1988) 513–886, https://doi.org/10.1063/1.555805.
[42] A.D. Bokare, W. Choi, Review of iron-free Fenton-like systems for activating H2O2 in advanced oxidation processes, J. Hazard. Mater. 275 (2014) 121–135, https://doi.org/10.1016/j.jhazmat.2014.04.054.
[43] N. Klamerth, N. Miranda, S. Malato, A. Agüera, A.R. Fernández-Alba, M.I. Maldonado, J.M. Coronado, Degradation of emerging contaminants at low concentrations in MWTPs effluents with mild solar photo-Fenton and TiO2, Catal. Today 144 (2009) 124–130, https://doi.org/10.1016/j.cattod.2009.01.024.
[44] I. Janik, D.M. Bartels, C.D. Jonah, Hydroxyl radical self-recombination reaction and absorption spectrum in water up to 350 °C, J. Phys. Chem. A 111 (2007) 1835–1843, https://doi.org/10.1021/jp065992v.